Effect of tea stalk biochar derived from pyrolysis at different temperatures on adsorption capacity of asphalt fume

Duan, Hao; Liu, Quantao; Mao, Sanpeng; He, Yanheng; Han, Xiaobin; Yu, Jianying; Xu, Shi

DOI
10.1016/j.conbuildmat.2025.141523

Publication date
2025

Document Version
Final published version

Published in
Construction and Building Materials

Construction and Building Materials 481 (2025) 141523

Contents lists available at ScienceDirect

Construction and Building Materials

journal homepage: www.elsevier.com/locate/conbuildmat

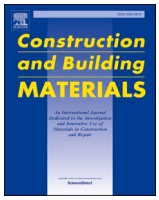

Effect of tea stalk biochar derived from pyrolysis at different temperatures on adsorption capacity of asphalt fume

Hao Duan [a], Quantao Liu [a], Sanpeng Mao [b], Yanheng He [a], Xiaobin Han [c], Jianying Yu [a,*], Shi Xu [d,e,**]

[a] State Key Laboratory of Silicate Materials for Architectures, Wuhan University of Technology, Wuhan 430070, PR China
[b] Research Institute of Petro China Fuel Oil Co., Ltd., Beiwucun Road 25, Beijing 100195, PR China
[c] School of Electric Power, Civil Engineering and Architecture, Shanxi University, Taiyuan 030031, PR China
[d] School of Civil Engineering and Architecture, Wuhan University of Technology, Luoshi Road 122, Wuhan 430070, PR China
[e] Faculty of Civil Engineering and Geosciences, Delft University of Technology, Stevinweg 1, Delft 2628 CN, the Netherlands

ARTICLE INFO

Keywords:
Asphalt
Tea stalk biochar
Microstructure
Adsorption
Fume

ABSTRACT

Asphalt fumes released at high temperatures significantly impact human health and the natural environment. This study systematically investigated the microstructure and compositional characteristics of tea stalk biochar (TB) from pyrolysis at different temperatures (300℃, 400℃, 500℃, and 600℃) and its adsorption capacity for asphalt fumes. Scanning electron microscopy and Brunauer-Emmett-Teller analysis indicated that increasing pyrolysis temperatures enhanced the porosity and BET surface area of TB, transitioning its structure from dense and low-porosity to highly porous. Fourier-transform infrared spectroscopy and elemental analysis revealed that higher temperatures promoted biochar graphitization, reduced oxygen-containing functional groups, and increased hydrophobicity and aromaticity. Analysis of asphalt fumes demonstrated that adding 1 % TB significantly reduced asphalt fume emissions, including VOCs, H_2S, SO_2, and NO_x. TB prepared at 500℃ (500TB) exhibited optimal adsorption, reducing VOCs by 68.6 % and H_2S by 87.5 %. GC-MS analysis further revealed that 1 % 500TB reduced aliphatic hydrocarbons, aromatic compounds, oxygen-containing compounds, and sulfur-containing compounds in asphalt VOCs by 63 %, 69 %, 67.2 %, and 63.3 %, respectively. The superior adsorption performance of 500TB was attributed to its larger surface area, diverse mesoporous structure, and high aromatic carbon content, enhancing its affinity for pollutants. Physical tests indicated that biochar enhances the thermal stability and deformation resistance of asphalt by increasing its softening point, viscosity, and penetration index, while maintaining acceptable ductility. These findings demonstrate the effectiveness of TB for mitigating asphalt fume emissions.

1. Introduction

Asphalt is the primary material used for highway and road paving due to its desirable properties, including smoothness, wear resistance, noise reduction, and ease of maintenance and repair [1–3]. However, during high-temperature processes such as production, transportation, and construction, asphalt releases harmful fumes containing volatile organic compounds (VOCs), hydrogen sulfide (H_2S), sulfur dioxide (SO_2), nitrogen oxides (NO_x), and particulate matter [4–7]. These emissions not only deteriorate air quality but also pose serious health risks, because many of the released compounds are toxic or potentially carcinogenic [8,9].

To address these risks, mitigating the emission of asphalt fumes has become a key area of research [10–12]. Various adsorption materials, such as porous materials, layered structures silicates, and nanomaterials, and so on, have been employed to mitigate asphalt fumes, but challenges remain. For instance, while adding 5 % activated carbon can reduce the release of most VOCs species from asphalt, it paradoxically increases the emission of certain VOCs species [13]. Materials such as layered double hydroxides (LDHs), diatomite, and attapulgite show effective VOCs adsorption only at high dosages (exceeding 4 % of asphalt mass) [14–16], which can impair the low-temperature performance of asphalt.

* Corresponding author.
** Corresponding author at: School of Civil Engineering and Architecture, Wuhan University of Technology, Luoshi Road 122, Wuhan 430070, PR China.
E-mail addresses: jyyu@whut.edu.cn (J. Yu), xushi@whut.edu.cn (S. Xu).

https://doi.org/10.1016/j.conbuildmat.2025.141523
Received 9 January 2025; Received in revised form 23 April 2025; Accepted 25 April 2025
Available online 5 May 2025

The adsorption efficiency of zeolites, such as ZSM-5, is influenced by their pore structure. As a result, ZSM-5 exhibits relatively low inhibition efficiency, with a maximum VOC reduction of 31.1 % [17,18]. Metal-organic frameworks (MOFs), like UiO-66, can reduce VOC emissions by 50.4 % at 0.6 % dosage, but their high cost and complex synthesis limit large-scale applications [19]. Moreover, most studies have yet to address the adsorption of gases like H_2S and NOx, which are important components of asphalt fume as the main source of unpleasant odors [20,21]. Given the limitations of existing adsorption materials, it is necessary to explore alternatives with improved adsorption capacity for asphalt fumes. Biochar is a porous material derived from biomass through thermochemical conversion, characterized by a high specific surface area, diverse pore structure, abundant surface functional groups, and adjustable structure, all of which enhance its adsorption capacity [22,23]. Compared to activated carbon, biochar is derived from agricultural waste, making it a more environmentally friendly alternative. In contrast to synthetic LDHs and zeolites, biochar offers a lower production cost.

Recently, biochar has shown significant potential in adsorbing persistent organic pollutants and heavy metals from soil and water [24–26]. For example, Krebsbach et al. [27] prepared poplar biochar at a pyrolysis temperature of 900°C. The results showed that when the biochar concentration was 0.1 g/L and the perfluorooctane sulfonate (PFOS) concentration was 500 μg/L, the biochar was able to remove 95 % of PFOS within 4 hours. Kayiranga et al. [28] investigated the adsorption capacity of bamboo biochar for thallium (Tl) in soil and found that bamboo biochar adsorbed 96.76 % of Tl within 15 minutes, significantly reducing Tl contamination in soil. Similarly, Wang et al. [29] used Phragmites australis biochar to adsorb phenanthrene from water, with a maximum equilibrium adsorption capacity of 1.97 mg/g, far exceeding that of activated carbon and modified bentonite. Zhang et al. [30] demonstrated the excellent adsorption performance of potassium ferrate-activated tea stalk biochar in removing Cu^{2+} and Zn^{2+} from wastewater, while Khalil et al. [31] reported that biochar derived from tea waste could remove 99.3 % of Cr^{6+} within 2 hours. However, the application of biochar in asphalt fume adsorption has not been studied.

Tea stalks, a byproduct of tea production, have shown a superior pore structure and larger specific surface area compared to other biochar materials [32]. China produces about 3 million tons of tea stalks annually, most are burned or composted [33,34], converting it into biochar with both environmental and economic benefits [35,36]. In this study, tea stalk biochar (TB) was prepared at various pyrolysis temperatures, and its structural and compositional properties were analyzed using scanning electron microscopy (SEM), Brunauer-Emmett-Teller (BET) analysis, elemental analysis (EA), and Fourier-transform infrared spectroscopy (FTIR). Then, TB was used to modify asphalt with the aim of reducing its fume emission. A photoionization detector (PID) was used to measure the concentrations of VOCs, H_2S, NOx, and SO_2 in biochar-modified asphalt fumes. Additionally, thermal desorption gas chromatography mass spectrometry (TD-GC-MS) was further used to evaluate the inhibitory efficiency of TB on different types of VOCs in asphalt. The experimental design and tests are illustrated in Fig. 1.

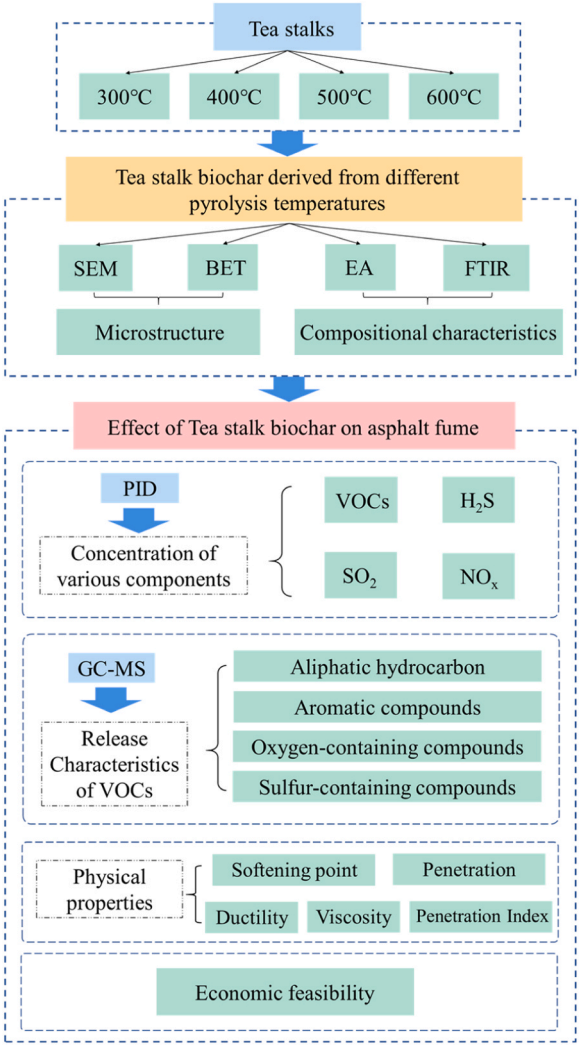

Fig. 1. Research process chart.

Fig. 2. Tie Guan Yin tea stalk.

2. Materials and methods

2.1. Materials

Tea stalks, from Tieguanyin tea, were collected from a local tea factory in Anxi, Quanzhou, China, as shown in Fig. 2.

The asphalt was provided by Petrochina Qinhuangdao Fuel Oil Asphalt Co., Ltd, China. The physical properties of the asphalt are shown in Table 1.

Table 1
Physical properties of asphalt.

Item	Test value	Test standard
Penetration (25℃, 0.1 mm)	76	ASTM D 5
Softening point (℃)	48.3	ASTM D 36
Viscosity (60℃, Pa·s)	221	ASTM D 2171
Ductility (15℃, cm)	60	ASTM D 113

2.2. Preparation of tea stalks biochar

First, the crushed tea stalks were passed through a 200-mesh sieve and placed in a ceramic dish. Seal the ceramic dish with tin foil and place

it in a muffle furnace. Under sealed and oxygen-free conditions, the temperature was increased at a rate of 15℃/min to 300℃, 400℃, 500℃, and 600℃ respectively. The tea stalks were then pyrolyzed at these temperatures for 2 hours and subsequently cooled to room temperature in a desiccator to obtain tea stalk biochar (TB). The biochar was labeled as XTB, where "X" corresponds to the pyrolysis temperature.

2.3. Characterization of TB

2.3.1. SEM

The morphology and structure of the biochar were analyzed using scanning electron microscope (FEG450 type, FEI Company of the United States) at a magnification of 10,000x. Before imaging, the biochar sample was coated with a thin layer of gold by sputtering for 30 seconds to enhance conductivity. The prepared sample was then placed on the test plate and secured with conductive adhesive for analysis.

2.3.2. BET

BET analysis was done with Micromeritics model-ASAP 2460, degassing conditions 150 °C, and for 12 h. The BET surface area of the biochar samples was determined using nitrogen adsorption-desorption isotherms. The micropore volume (pores <2.0 nm in diameter) and the corresponding surface area were calculated using the t-plot technique. To estimate the total pore volume of each biochar sample, the adsorbed quantity (g) was converted into liquid nitrogen volume based on a density of 0.808 g/mL at atmospheric pressure near saturation. The average pore diameter of each biochar sample was then calculated using formula 1:

$$\text{Average pore diameter} = \frac{4 \times V_t}{S_{BET}} \quad (1)$$

Where:

V_t represents the total pore volume

S_{BET} denotes the BET surface area

2.3.3. EA

The increase in pyrolysis temperature accelerates the carbonization process of biomass, thereby affecting the elemental composition and chemical properties of biochar. To investigate the influence of the elemental composition of TB on its adsorption of asphalt fumes, this study used an elemental analyzer (Vario EL cube, Germany) to determine its carbon, hydrogen, nitrogen, and sulfur contents. The principle of analysis was dynamic adsorption-procedural desorption-TCD detection. The content of the oxygen element was obtained using the subtraction method: O%= 100 % - (C + H + N + S + ash, %). The ash content, representing the number of inorganic substances, was determined by heating the biochar samples in a muffle furnace at 750℃ for 6 hours, and the final value of ash is the average of three tests.

2.3.4. FTIR

FTIR is a commonly used spectroscopic technique that provides information about molecular structure and chemical bonds by measuring the absorption of different infrared wavelengths. In this study, the infrared spectra of different biochars were tested using the potassium bromide pellet method to analyze their functional groups and chemical structure. The characteristic absorption peaks of TB were analyzed using the FTIR spectrometer (Frontier, PerkinElmer, America) in the wavenumber range of 400–4000 cm^{-1} , with 32 scans per sample and a resolution of 4 cm^{-1} .

2.4. TB-modified asphalt preparation and physical properties test

The preparation process of TB-modified asphalt (TB-A) was as follows. First, 200 g of base asphalt was poured into a three-necked flask and heated in an oil bath, maintaining the asphalt temperature at 160℃. Then, 2 g (1 % of the weight of asphalt) of TB was added to the hot asphalt. The opening of the flask was closed, and the rotation speed was set to 300 rpm. After stirring for 1 hour, TB-A was prepared. For convenience, different tea stalk biochar-modified asphalts are referred to as XTB-A, where 'X' represents the pyrolysis temperature.

The penetration, softening point, 15℃ ductility, and 60℃ viscosity of the biochar-modified asphalt were tested according to ASTM D 5, ASTM D 36, ASTM D 113, and ASTM D 2171, respectively.

2.5. Asphalt fumes testing

2.5.1. Analysis of asphalt fume components

The asphalt fumes are primarily consisting of volatile organic compounds (VOCs), nitrogen oxides (NO_x), sulfur dioxide (SO_2), and hydrogen sulfide (H_2S). In this study, the main component contents of asphalt fumes were first analyzed. Photoionization detector (PID; Korno GT-1000, China) gas detector was used, set to a four-channel detection mode to separately measure the contents of VOCs, H_2S, NO_x, and SO_2. The fume detection ranges were as follows: VOCs: 0–2000 ppm, H_2S, and SO_2: 0–200 ppm, NOx: 0–500 ppm, with a resolution of 0.1 ppm. The testing method is shown in Fig. 3: After preparing TB-A, place it in a three-neck flask. Then, turn on the air pump, place the fume storage bottle in an ice-water bath, and use a PTFE filter to remove particles. The asphalt fume is drawn from the bottle through the PID. The detection time is set to 3 minutes, and the maximum value recorded during this period is noted. Test each sample three times under the same conditions and take the average to obtain the final result.

The working principle of the PID used for asphalt fumes detection is based on its internal vacuum ultraviolet (UV) light source. This high-energy light irradiates pollutant molecules present in the asphalt fumes, breaking them down into positively charged organic ions and negatively charged electrons. These charged fragments generate a current between two electrodes, with the intensity of the current reflecting the concentration of the corresponding substances. The detector amplifies this current and converts it into concentration values, which are ultimately displayed in parts per million (ppm). Using this principle, the PID can sensitively detect the concentration of pollutant in asphalt fumes. The detection mechanism is illustrated in Fig. 4.

2.5.2. Analysis of VOCs components in asphalt fume

Volatile organic compounds (VOCs) encompass a broad range of compounds, primarily including non-methane hydrocarbons (such as alkanes, alkenes, alkynes, and aromatics), oxygenated organic compounds (aldehydes, ketones, alcohols, ethers, etc.), halogenated hydrocarbons, nitrogen-containing compounds, and sulfur-containing compounds. To determine the effect of TB on each VOC component released from asphalt, Thermal desorption gas chromatography mass spectrometry (TD-GC-MS; Agilent 7890B-5977B, USA) was used to analyze the composition of asphalt fume. The procedure for collecting fume is as follows: (1) The asphalt sample is placed in a sealed three-neck flask and heated to 160℃, with a temperature hold for 30 minutes. (2) The valve of the three-neck flask is then opened, and a sampling pump is employed to transfer the flue gas into an adsorption column (Agilent 222–5532LTM) at a flow rate of 500 mL/min for a duration of 10 seconds. (3) After the flue gas collection is completed, the adsorption column is inserted into a GC-MS system for the analysis of the collected gas components.

The workflow of the TD-GC-MS is as follows: (1) Asphalt fume is adsorbed onto a sorbent tube and captured at an ultra-low temperature of −150℃ using high-purity N_2 as the carrier gas (flow rate: 60 mL/min) for 5 minutes. (2) The captured gas is then rapidly heated to 120℃ to desorb the flue gas, with a desorption time of 5 minutes. (3) The desorbed gas is analyzed by gas chromatography-mass spectrometry (GC-MS). The composition and concentration of different substances in the separated gas are determined. The temperature program for GC-MS is set to 72℃ for 4 minutes, followed by an increase at a rate of 8.0℃/min to

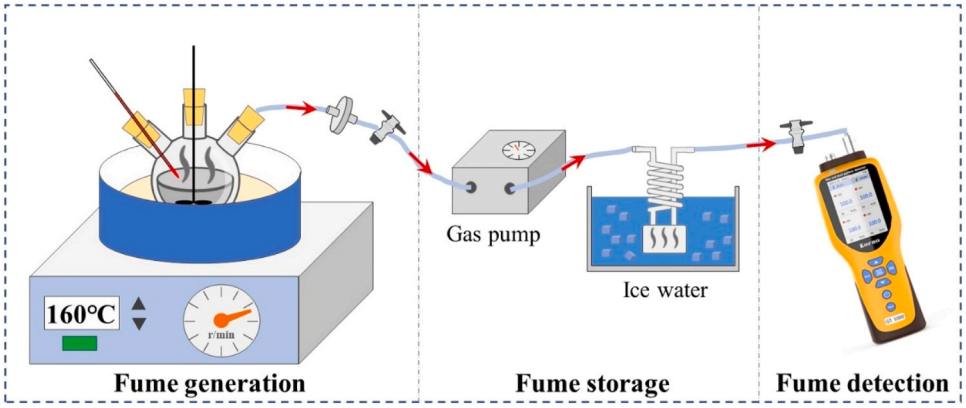

Fig. 3. Fume-generation and detection device for asphalt.

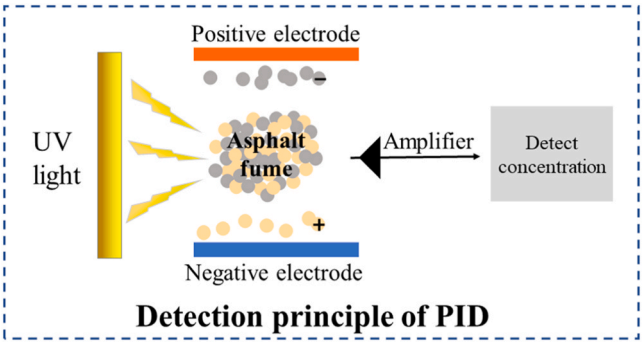

Fig. 4. Detection principle of PID for asphalt fume.

280℃, where it is held for 2 minutes.

3. Results and discussion

3.1. Structure and composition characterization of TB

3.1.1. Microstructure

SEM images of 300TB, 400TB, 500TB, and 600TB were presented in Fig. 5, respectively. As the pyrolysis temperature increased, the microstructure of TB underwent significant changes. In Fig. 4(a), the microstructure of 300TB exhibited a dense surface with few visible pores, which was attributed to incomplete pyrolysis at this lower temperature. This led to greater retention of the original biomass structure and limited pore formation. As the pyrolysis temperature rose to 400℃, visible pore structures began to develop within the biochar, though the overall structure remained relatively compact. At the higher temperature of 500℃, shown in Fig. 4(c), the biochar surface exhibited a looser, more

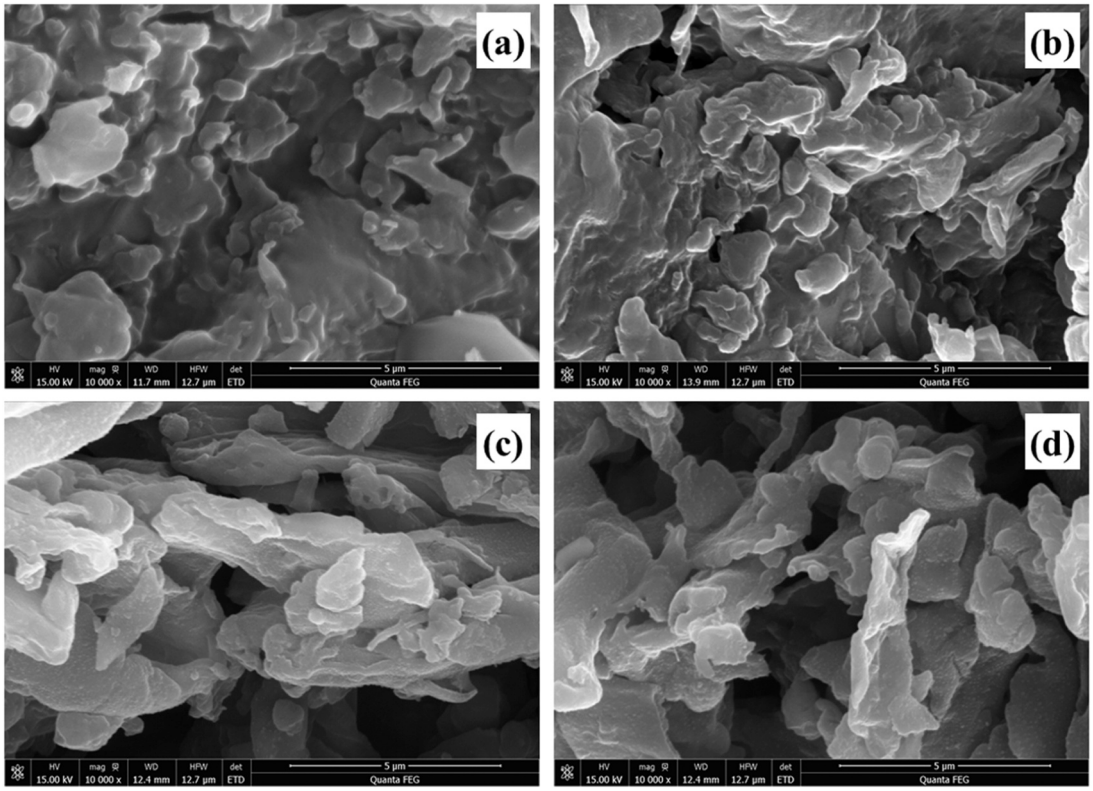

Fig. 5. SEM images of TB derived from different pyrolysis temperatures (a. 300TB, b. 400TB, c. 500TB, d. 600TB).

porous structure. This increase in porosity was attributed to the greater volatilization of organic components in the tea stalks at elevated temperatures, promoting a more developed micro- and mesoporous structure. Finally, at a pyrolysis temperature of 600℃, further decomposition of biomass occurred, producing an abundance of pores. As shown in Fig. 4(d), the biochar surface became even looser, with higher porosity and a more complex pore structure.

3.1.2. Pore analysis

The pore structural properties of biochar produced at various pyrolysis temperatures were characterized using nitrogen adsorption isotherms at 77 K. As shown in Fig. 6, all biochars exhibited similar adsorption isotherm shapes, which were classified as Type IV isotherms according to IUPAC standards. At low relative pressures (0–0.1), the adsorption volume increased slowly, indicating monolayer adsorption. As the relative pressure increased to moderate levels (0.1–0.9), a plateau formed, signifying multilayer adsorption within the biochar structure. When the relative pressure reached 0.9, the adsorption curve showed a sharp rise, suggesting the presence of numerous large pores and structural cracks in the biochar, resulting in a sudden increase in nitrogen adsorption capacity.

A distinct separation between the adsorption and desorption branches was observed at moderate and high relative pressures, revealing a hysteresis loop characteristic of mesoporous and macroporous structures. This hysteresis loop confirmed the presence of a well-developed porous structure in the TB. For the biochar produced at 300℃ (300TB), the hysteresis loop was relatively small but became more pronounced as pyrolysis temperatures increased, indicating a transition toward a more developed mesoporous and macroporous structure. In the 500TB and 600TB samples, the adsorption and desorption curves did not form a closed loop at low pressure, indicating the presence of not only mesopores and macropores but also a certain number of micropores within the biochar structure. During the adsorption process in the micropores, as pressure increased, the interlayer spacing of layered compounds within the biochar gradually expanded, allowing nitrogen to enter micropores that were previously inaccessible. This phenomenon, known as intercalation, occurred within the biochar. The interlayer spacing was close to the pore size of the micropores, making it difficult for the adsorbate trapped between the layers to escape. Even at relatively low pressure, nitrogen remained trapped in these pores, preventing the isotherm from closing.

The hysteresis loop was further classified as Type H3, indicating that the pores within the TB were likely irregular, slit-like, or plate-like in nature. The increased prominence of the hysteresis loop at higher pyrolysis temperatures implies that thermal treatment facilitated the development of these irregular, open slit-like pores, potentially enhancing the BET surface area and adsorption capacity of biochar.

Fig. 7 showed the pore size distribution curves of TB derived from different pyrolysis temperatures. Each curve indicated the distribution of pore volume as a function of pore width. These curves revealed substantial differences in porosity among samples exposed to varying pyrolysis conditions. In the 300TB sample, the pore volume distribution exhibited a pronounced peak around 13.98 nm, suggesting that the pores were primarily mesoporous (in 2–50 nm range). The overall curve indicated limited pore development, with relatively low pore volume across the measured width range. This result was consistent with incomplete pyrolysis at low temperatures, leading to a more compact structure and less effective pore formation. In the 400TB sample, the

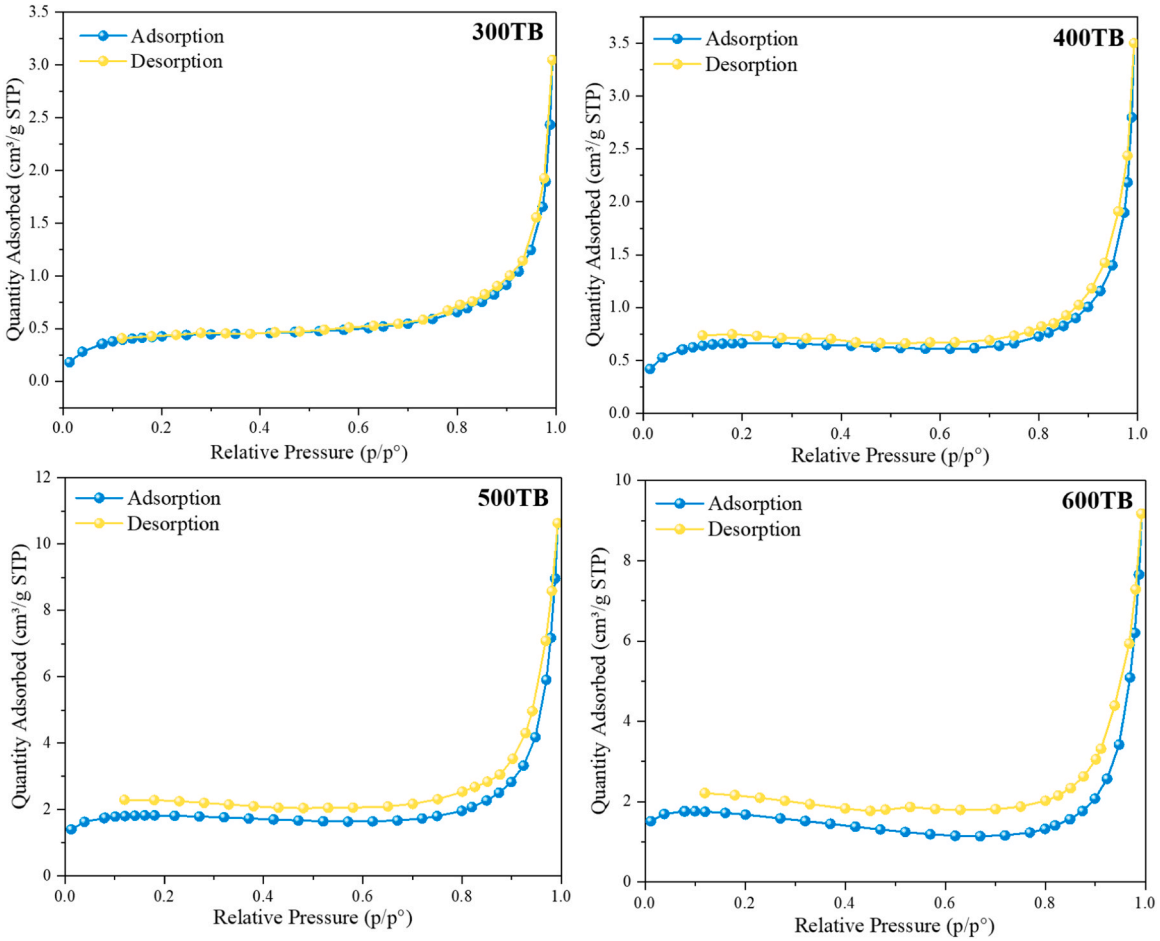

Fig. 6. Isothermal adsorption-desorption curves of TB derived from different pyrolysis temperatures.

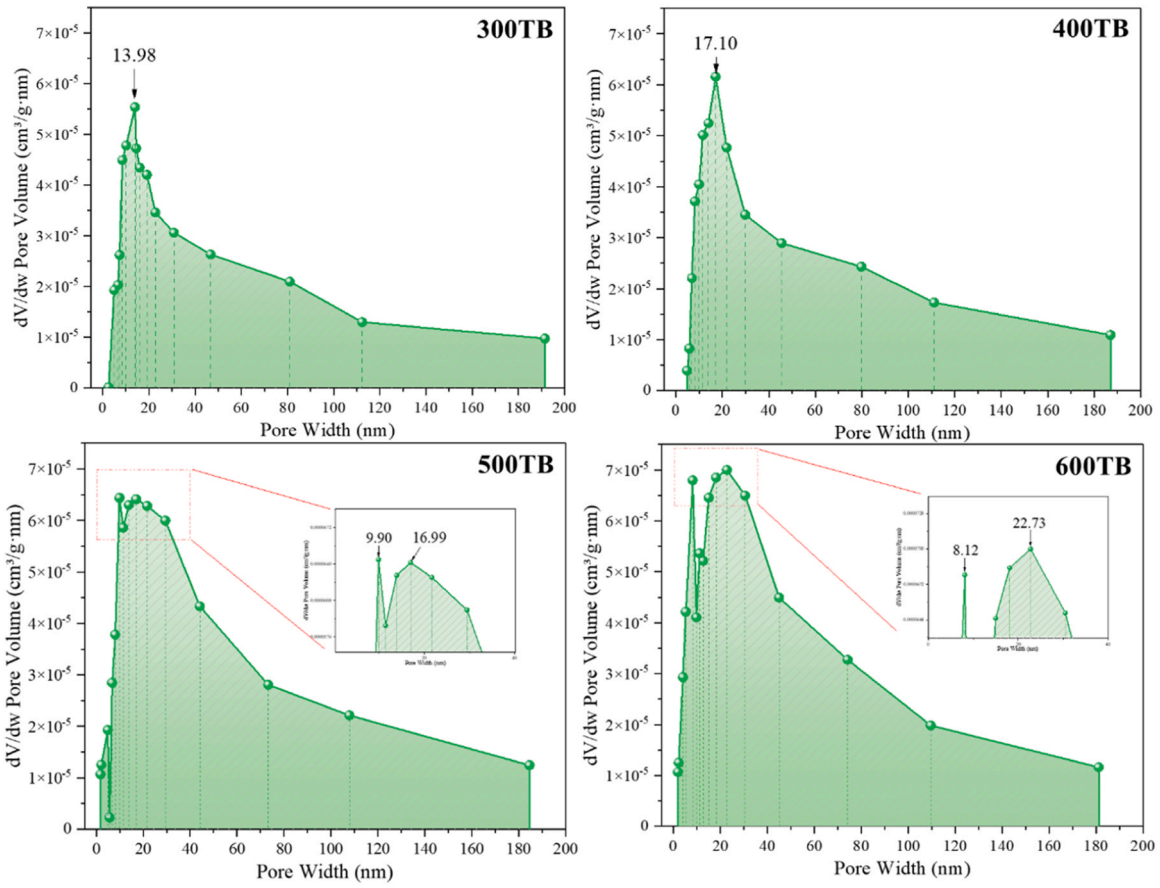

Fig. 7. Pore size distribution of TB derived from different pyrolysis temperatures.

peak shifted to 17.10 nm, and the proportion of smaller pores increased compared to the 300TB sample. This change in porosity was attributed to the increased volatilization of organic matter at this temperature, which formed some smaller pores.

At 500℃, the pore structure of the biochar became notably more complex, with the primary peak broadening and two distinct peaks appearing at 9.90 nm and 16.99 nm, respectively. This pattern indicated a more intricate pore network within the biochar, comprising a mixture of pore sizes. The broad mesopore size distribution suggests that biochar produced at this temperature may be more versatile in adsorbing contaminants of various sizes, effectively capturing both smaller and larger molecules. Similarly, when the pyrolysis temperature was elevated to 600℃, the main peak widened further, with prominent peaks observed at 8.12 nm and 22.73 nm. The peak at 22.73 nm reflected an expansion in the pore structure of 600TB, resulting in a higher proportion of larger pores. The observed changes in pore structure in both 500TB and 600TB were attributed to the higher pyrolysis temperature, which promoted the decomposition of more organic materials, leading to the formation of a highly porous structure with both small and large mesopores. This structure appeared notably loose and porous, with a well-developed interconnected pore network.

In summary, as the pyrolysis temperature increased, the biochar underwent a progressive structural transformation. Lower temperatures (300℃ and 400℃) resulted in a denser structure with lower pore content attributed to the incomplete volatilization of organic compounds. At higher temperatures (500℃ and 600℃), the biochar developed a more open and porous structure, reflecting enhanced pore formation as a result of more extensive organic decomposition.

Table 2 presented the BET surface area, average pore size, and micropore area of TB at different pyrolysis temperatures. As the pyrolysis temperature increased, the specific surface area of the biochar increased significantly, with 600TB reaching 6.99 m^2/g, a substantial improvement compared to 1.52 m^2/g for 300TB. Similarly, the micropore area increased as the pyrolysis temperature rose, from 0.38 m^2/g to 5.56 m^2/g, indicating that higher pyrolysis temperatures promoted the development of more microporous structures. In contrast, the average pore size decreased from 12.38 nm at 300℃ to 8.11 nm at 600℃, reflecting the contraction of pore sizes and structural optimization. The increase in micropore area and reduction in pore size demonstrated the significant influence of pyrolysis temperature on the porosity characteristics of TB. The Biochar prepared at 500°C and 600°C exhibited a larger specific surface area and a more developed microporous structure.

Table 2
BET analysis results of TB derived from different pyrolysis temperatures.

	300TB	400TB	500TB	600TB
BET Surface Area (m^2/g)	1.52	2.39	6.93	6.99
Average pore width (nm)	12.38	9.12	8.78	8.11
Micropore area (m^2/g)	0.38	1.72	4.31	5.56

3.1.3. *Element analysis*

Fig. 8(a) presented the elemental composition of TB at various pyrolysis temperatures. The pyrolysis temperature significantly affected the elemental composition of the biochar. As the pyrolysis temperature rose, the carbon (C) content increased, while the hydrogen (H) and oxygen (O) contents decreased. This alteration was likely due to dehydration reactions involving the cellulose, hemicellulose, and lignin in the tea stalk precursors during pyrolysis, resulting in the substantial loss of O and H, as well as the production of CO_2 and some loss of C. However, the overall loss of O and H was more pronounced.

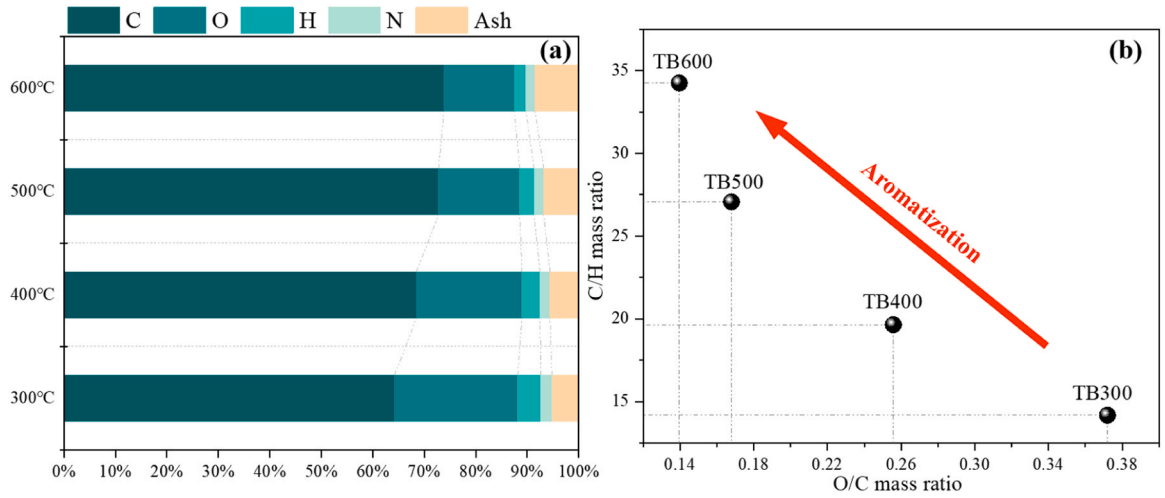

Fig. 8. Elemental analysis results of TB derived from different pyrolysis temperatures.

As the pyrolysis temperature increased from 300℃ to 600℃, the C content rose by 10.82 %. This increase was attributed to the enhanced cleavage of long-chain aliphatic groups at higher temperatures, leading to a greater rate of volatile component loss. The prolonged exposure to elevated temperatures facilitated the thermal cleavage of C-H bonds, resulting in a reduction of H content, thereby increasing the degree of carbonization of the tea stalk and resulting in the formation of a more stable aromatic carbon structure. As the pyrolysis temperature continued to rise, the weaker bonds within the tea stalk broke, and the O- and H-containing functional groups in the biochar were progressively removed, leading to a significant reduction in oxygen and hydrogen contents. Notably, when the pyrolysis temperature reached 600℃, the oxygen content was reduced by 13.14 %. Below 500℃, the decrease in O and H was more pronounced; however, when the pyrolysis temperature increased from 500℃ to 600℃, the reduction in O and H was less marked, indicating that the volatile organic compounds and other constituents within the tea stalk underwent a multistep degradation process.

The O/C and C/H ratios were crucial indices for assessing the stability and degree of oxidation of biochar. Fig. 8(b) showed the O/C and C/H ratios of four types of TB. The O/C and C/H ratios of TB ranged from 0.37 to 0.14 and 14.17–34.25, respectively. As the pyrolysis temperature increased, the O/C ratio gradually decreased, while the C/H ratio progressively increased, indicating higher aromaticity of the biochar. A higher O/C ratio suggested that, at lower pyrolysis temperatures, biochar contained more oxygen-containing functional groups, such as hydroxyl, carboxyl, and ketone groups. At elevated temperatures, aromatization reactions became more prominent, leading to the formation of ring structures with C-C bonds or π-conjugated ring structures. For instance, at 600℃, the C/H ratio of biochar reached 34.25, implying that at this temperature, carbon atoms in the biochar primarily bonded in ring structures, resulting in greater stability. Additionally, the increase in carbon content typically reduced the polarity of the material, thereby enhancing its hydrophobic and oleophilic properties [37,38], which was beneficial for its dispersion in asphalt.

3.1.4. Functional group analysis

Fig. 9 presented the FTIR spectra of the tea stalk and TB derived from different pyrolysis temperatures. A strong and broad absorption band attributed to the stretching vibration of -OH was observed around 3400 cm^{-1} in the FTIR spectra of the tea stalk. This peak gradually diminished with rising temperatures and became negligible at 600℃, indicating the depletion of -OH groups. The stretching vibration peak of C-H, located around 2800–3000 cm^{-1} , was more pronounced in the tea stalk and 300TB, suggesting a higher content of fatty hydrocarbons at lower temperatures. Additionally, peaks corresponding to C═O

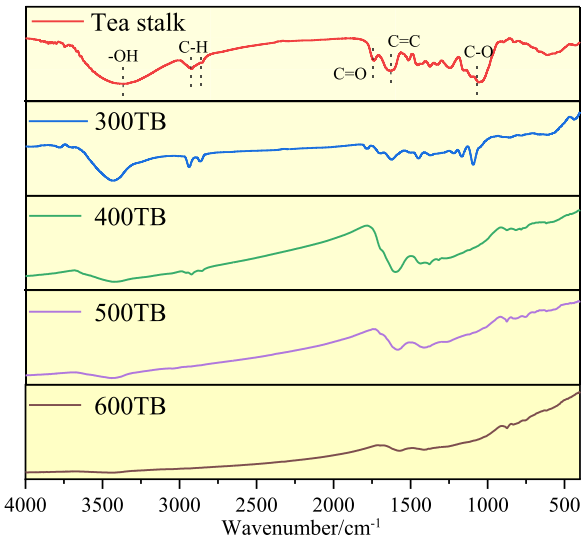

Fig. 9. FTIR of tea stalk and TB derived from different pyrolysis temperatures.

stretching vibrations (1700–1750 cm^{-1}) and C═C stretching vibrations (1600 cm^{-1}) were identified. Peaks between 1000–1200 cm^{-1} were attributed to the C-O stretching vibrations of oxygen-containing groups.

As the pyrolysis temperature increased, the intensities of these peaks decreased due to depolymerization and dehydration processes. Notably, significant changes in FTIR peaks began to occur at 400℃, marking the onset of major structural transformations. These modifications in functional groups throughout the pyrolysis process were predominantly characterized by a decrease in aliphatic carbon and a relative increase in aromatic carbon, reflecting the progressive carbonization and stabilization of the biochar structure. Among the analyzed samples, the FTIR spectra of the tea stalk and 300TB were the most similar, while higher temperatures induced significant alterations in the functional groups.

3.2. Effect of TB on asphalt fume

3.2.1. Concentration of various components in asphalt fume

During the mixing, transportation, and paving processes of asphalt mixtures, the asphalt must be heated to maintain a fluid state. This heating process causes the release of various volatile molecules, and as the temperature increases, the amount of smoke and vaporized compounds also rises. In this study, a PID gas detector was used to measure

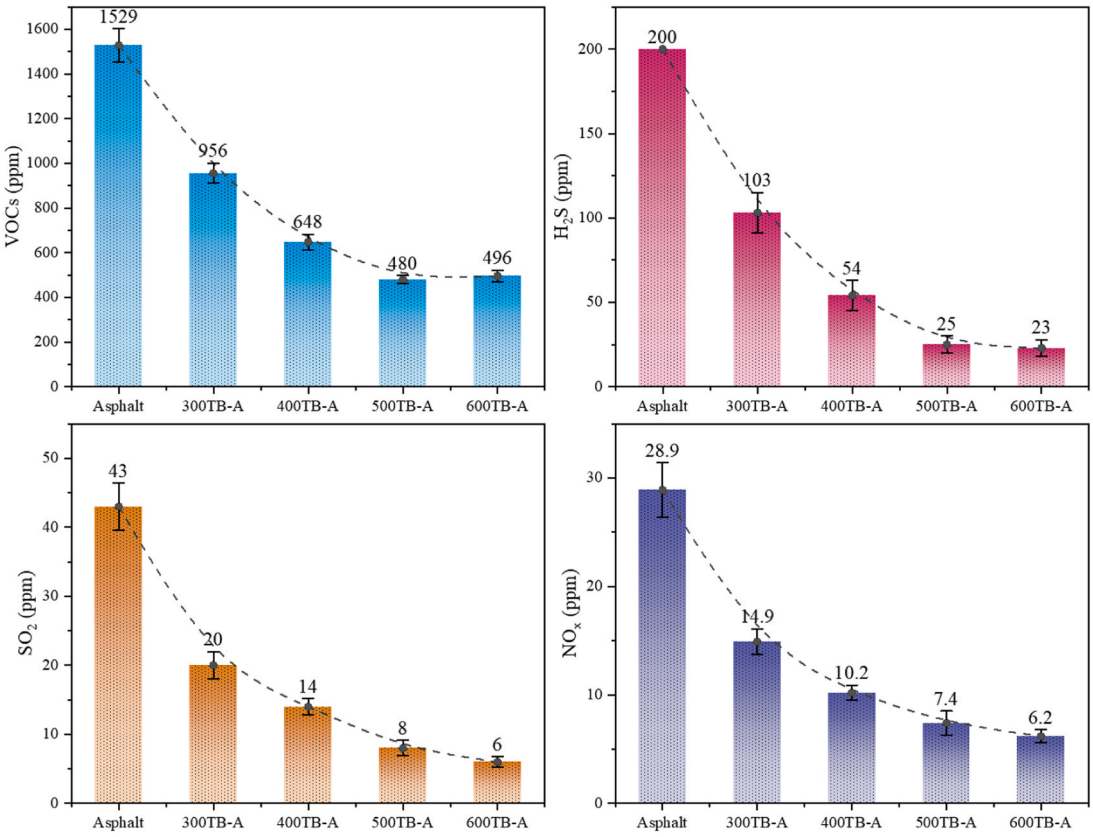

Fig. 10. Influence of TB on various components in asphalt fume.

the concentrations of VOCs, H_2S, NO_x, and SO_2 emitted from asphalt at 160℃, with the results shown in Fig. 10.

Fig. 10 showed that the base asphalt without TB has a high level of pollutants, with VOCs concentration reaching 1529 ppm, H_2S concentration hitting the detection limit of the instrument (200 ppm), and SO_2 and NO_x concentrations of 43 ppm and 29 ppm, respectively. After the addition of TB, the concentrations of all pollutants significantly decreased. When 1 % of 300TB was added, the VOCs in 300TB-A dropped to 956 ppm, H_2S to 103 ppm, and SO_2 and NO_x to 20 ppm and 15 ppm, respectively. As the pyrolysis temperature increased, the effectiveness of TB in reducing asphalt emissions was improved. At a pyrolysis temperature of 500℃, the concentrations of the four pollutants in 500TB-A were 480 ppm, 25 ppm, 8 ppm, and 7 ppm, respectively, reflecting a 68.6 % reduction in VOCs, and at least a 87.5 % reduction in hydrogen sulfide, an 81.4 % reduction in sulfur dioxide, and a 75.9 % reduction in nitrogen oxides. This effectiveness was attributed to the excellent pore structure and composition of 500TB. Its high specific surface area provided more adsorption sites, and the pore size distribution, including small and medium mesopores, enhances the ability of 500TB to adsorb pollutants of various sizes. The more aromatic π-π conjugated structure facilitates the capture of aromatic pollutants, while increased hydrophobicity aids in the dispersion of biochar in asphalt. Under these combined effects, 500TB exhibited effective fume suppression capabilities. At a pyrolysis temperature of 600℃, although 600TB also effectively suppressed asphalt fumes, its VOC suppression ability is slightly lower than that of 500TB. This may be because although the porosity of biochar increases at higher pyrolysis temperatures, the original chemical structure of the tea stalks is more thoroughly degraded, leading to excessive loss of functional groups. These functional groups play a crucial role in chemical adsorption and surface interactions, and their depletion results in lower affinity for certain pollutants.

Overall, as the pyrolysis temperature increased, TB exhibited enhanced adsorption capacity and pollutant removal efficiency, particularly for VOCs and H_2S. This was because higher temperatures further increase the specific surface area and porosity, the internal pore structure of TB becomes more organized and complex, especially above 500℃.

3.2.2. *Release characteristics of VOCs from asphalt fume*

Fig. 11 showed the GC-MS analysis results of base asphalt and TB-A. In the chromatogram, each peak corresponded to a specific compound.

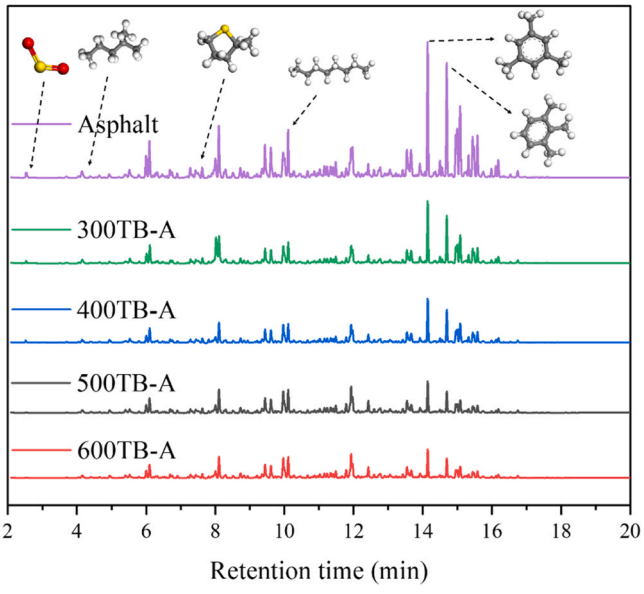

Fig. 11. GC-MS results of base asphalt and TB-A.

By comparing these peaks with reference data from a mass spectral library, the compounds were identified, facilitating the qualitative analysis of VOCs in the asphalt fumes. The height of each peak reflects the concentration of the corresponding compound, allowing for quantitative analysis through comparison of peak intensities. As illustrated in Fig. 11, the peak intensities of volatiles emitted from base asphalt were markedly higher than those from TB-A, indicating that the addition of TB effectively reduced the concentration of volatile compounds. The identified compounds were further classified by chemical structure and functional group into four categories: aliphatic hydrocarbons (AH), aromatic compounds (AC), oxygen-containing compounds (OC), and sulfur-containing compounds (SC). Fig. 12 presented several representative pollutant components found in the VOCs of asphalt.

Table 3 provided the analytical results on the effect of TB on the components of VOCs in asphalt fumes, while Fig. 13 illustrated the influence of TB on the number of VOCs types in asphalt fume. The analysis revealed that AH and AC constitute the primary components of asphalt VOCs, whereas OC and SC were relatively minor constituents. TB samples prepared at different pyrolysis temperatures exhibited significant differences in their microstructure and compositional characteristics, which directly impacted their pollutant adsorption capabilities. In base asphalt, a total of 91 pollutants were identified, including 58 types of AH, 23 types of AC, 6 types of OC, and 4 types of SC. The TB sample prepared at 300°C (300TB) demonstrated an initial adsorption capacity, reducing the number of VOC types in 300TB-A by 19, specifically lowering AH types by 11, AC by 4, OC by 2, and SC by 2. Although the pore structure of 300TB was not yet fully developed, it exhibited basic adsorption properties. As the pyrolysis temperature increased, the pore structure of TB gradually optimized, leading to further reductions in pollutant types in asphalt fumes. For 400TB-A, the number of VOCs was reduced by 23, with reductions of 15 types of AH, 4 types of AC, 2 types of OC, and 2 types of SC. At a pyrolysis temperature of 500℃, the biochar structure was further enhanced, with a significant increase in BET surface area and providing more adsorption sites for pollutants. The increased number of micropores and mesopores allowed for better capture and adsorption of pollutants with various molecular sizes. Consequently, the total number of VOCs types in 500TB-A was reduced by 29, with 20 fewer types of AH, 6 fewer types of AC, 1 less type of OC, and 2 fewer types of SC. Raising the pyrolysis temperature to 600°C resulted in a total reduction of VOCs in 600TB-A by 27, with reductions of 18 types of AH, 7 types of AC, 1 type of OC, and 1 type of SC. Compared to 500TB, the 600TB exhibited slightly reduced adsorption capacity for AH and SC, but an enhanced ability to adsorb AC. This effect may be attributed to the highly aromatic structure of 600TB, which increased its affinity for AC compounds, while the larger pore sizes slightly reduced its effectiveness in adsorbing smaller molecular pollutants.

Table 4 provided quantitative analysis results of pollutants obtained by integrating peak areas in the chromatograms. The data indicated that aliphatic hydrocarbons (AH) and aromatic compounds (AC) are the predominant pollutants in asphalt fumes, collectively accounting for approximately 90 % of total emissions. As shown in Fig. 13, the number of AH compounds is 2.52 times greater than that of AC compounds. However, in terms of total emission volume, AC contributed more substantially to the overall pollution load, highlighting its significant role in the emission profile of asphalt fumes.

Using the VOCs emissions from base asphalt as a reference, the inhibition rates of TB on various components were calculated based on the emission data for each sample, as shown in Fig. 14. The results indicate that 300TB showed limited inhibition of AH and AC, though it exhibited slightly higher inhibition rates for OC and SC compounds. With further optimization of pore structure at higher pyrolysis temperatures, 400TB demonstrated improved inhibition rates across all VOC components.

When the pyrolysis temperature reached 500℃, the inhibition efficiency of TB significantly enhanced, particularly for AH and AC. This improvement can be attributed to the substantial increase in the BET surface area of 500TB compared to 400TB, which provided more adsorption sites, thereby enhancing its adsorption capacity for pollutants. Furthermore, the more intricate pore structure of 500TB facilitated the adsorption of pollutants of various molecular sizes and properties. In contrast, the inhibition effect of 600TB was slightly lower than that of 500TB, although it displayed enhanced efficiency in adsorbing AC. This may be because, compared to 500TB, 600TB contains larger pore structures, allowing some smaller VOC molecules to escape, thereby reducing its effectiveness in restricting smaller molecules. Additionally, the higher pyrolysis temperature leads to more complete degradation of functional groups in tea stalks, negatively affecting asphalt fume adsorption. However, its highly aromatic structure and enhanced π-π

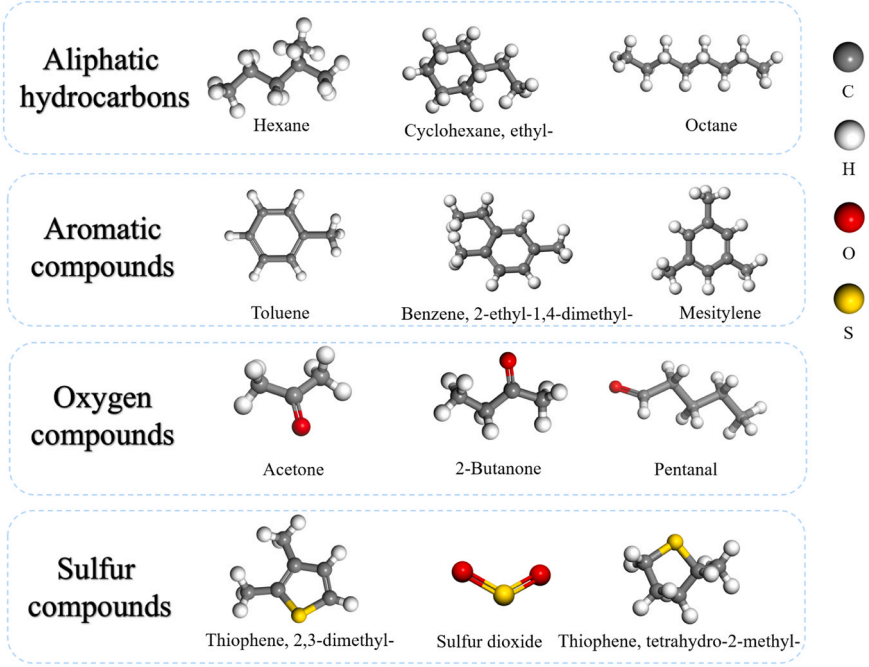

Fig. 12. Ball stick model of typical asphalt fume pollutants.

Table 3
Effect of TB on the components of VOCs in asphalt fume.

Types	IUPAC Name	Asphalt	300TB-A	400TB-A	500TB-A	600TB-A
AH	Butane, 2-methyl-	√	/	/	/	/
	Pentane	√	√	√	√	√
	Pentane, 2-methyl-	√	√	√	√	√
	Pentane, 3-methyl-	√	√	√	/	/
	n-Hexane	√	√	√	√	√
	Hexane, 2-methyl-	√	√	√	√	√
	Hexane, 3-methyl-	√	√	√	√	√
	Heptane	√	√	√	√	√
	Heptane, 2-methyl-	√	√	√	√	√
	Heptane, 3-methyl-	√	√	√	√	√
	Heptane, 2,6-dimethyl-	√	√	√	√	√
	Heptane, 2,3-dimethyl-	√	√	√	√	√
	Heptane, 2,4-dimethyl-	√	√	√	/	/
	Heptane, 3-ethyl−2-methyl-	√	√	√	√	√
	Octane	√	√	√	√	√
	Octane, 3-methyl-	√	√	√	√	√
	Octane, 2,6-dimethyl-	√	/	√	√	√
	Nonane	√	√	√	√	√
	Nonane, 4-methyl-	√	√	√	√	√
	Undecane	√	√	√	√	√
	Heptadecane, 7-methyl-	√	√	√	/	/
	Decane, 4-methyl-	√	√	√	√	√
	2-Pentene, (*E*)-	√	/	/	/	/
	2-Butene, 2-methyl-	√	/	√	/	/
	1-Pentene, 2-methyl-	√	√	√	√	√
	1-Hexene	√	√	/	/	/
	1-Hexene, 4-methyl-	√	√	√	√	√
	1-Hexene, 2-methyl-	√	√	/	√	√
	2-Hexene, (*Z*)-	√	/	√	/	/
	3-Hexene, (*Z*)-	√	√	√	√	√
	2-Butene, 2,3-dimethyl-	√	/	√	/	/
	1-Heptene	√	√	√	√	√
	2-Heptene, (*E*)-	√	√	/	√	√
	2,4-Heptadiene, (*E*,*E*)-	√	√	√	√	√
	3-Heptene, 2-methyl-, (*E*)-	√	/	/	/	/
	2-Octene, (*Z*)-	√	/	/	/	/
	1-Nonene	√	/	/	/	/
	1-Octene, 3,7-dimethyl-	√	√	√	√	√
	1-Heptene, 2,6-dimethyl-	√	√	√	√	√
	Cyclopropane, ethyl-	√	√	√	√	√
	Cyclopentane, methyl-	√	√	√	√	√
	Cyclopentane, ethyl-	√	√	√	√	√
	Cyclopentane, 2-ethylidene−1,1-dimethyl-	√	√	√	√	√
	Cyclohexane, methyl-	√	√	√	√	√
	Cyclohexane, ethyl-	√	√	√	√	√
	Cyclohexane, 1,1,3-trimethyl-	√	√	√	√	√
	Cyclohexane, 1,1,2,3-tetramethyl-	√	√	/	/	/
	Cyclopropane, 1-(1,1-dimethylethyl)−2-methylene-	√	√	/	/	√
	Cyclohexane, methylene-	√	/	√	√	√
	Cyclopentene, 4-methyl-	√	√	/	/	/
	Cyclopentene, 1-methyl-	√	√	/	/	/
	Cyclopentene, 4,4-dimethyl-	√	/	√	√	√
	Cyclohexene	√	√	/	/	√
	Cyclohexene, 4-methyl-	√	√	√	√	√
	Cyclohexene, 1-methyl-	√	√	√	√	√
	cis−1-Butyl−2-methylcyclopropane	√	√	/	/	/
	Cyclohexanone, 2,3-dimethyl-	√	√	√	/	/
	1,3-Pentadiene, 2-methyl-/	√	√	/	/	/
AC	1,3-Dimethyl−1-cyclohexene	√	/	/	/	/
	Benzene	√	√	√	√	√
	Toluene	√	√	√	√	√
	Benzene, 1,3-dimethyl-	√	√	√	√	√
	Benzene, 1,2,3-trimethyl-	√	√	√	√	√
	Benzene, propyl-	√	√	√	√	√
	Benzene, 1-ethyl−3-methyl-	√	√	√	√	√
	Mesitylene	√	√	√	√	√
	Benzene, 1-ethyl−2-methyl-	√	√	√	√	√
	Benzene, (2-methylpropyl)-	√	/	/	/	/
	Benzene, (1-methylpropyl)-	√	/	/	/	/
	p-Xylene	√	√	√	√	√
	p-Cymene	√	√	√	/	/
	o-Cymene	√	√	√	√	/
	Benzene, 1,2-diethyl-	√	√	√	√	√
	Benzene, 1-methyl−3-propyl-	√	√	√	√	√

(*continued on next page*)

Table 3 (*continued*)

Types	IUPAC Name	Asphalt	300TB-A	400TB-A	500TB-A	600TB-A
	Benzene, 1-ethyl−3,5-dimethyl-	√	√	/	/	/
	Benzene, 1,2-diethyl-	√	√	√	√	√
	Benzene, 1-methyl−4-propyl-	√	√	√	√	√
	Benzene, 2-ethyl−1,4-dimethyl-	√	√	√	√	√
	Benzene, 1,2,4,5-tetramethyl-	√	√	√	√	√
	Benzene, 1,2,3,4-tetramethyl-	√	√	√	√	√
	Benzene, 2-ethenyl−1,4-dimethyl-	√	/	/	/	/
OC	Acetone	√	√	√	√	√
	Butanal	√	√	√	√	√
	Pentanal	√	/	/	√	√
	Hexanal	√	√	√	√	√
	2-Butanone	√	/	/	/	/
	Cyclohexanone, 2,3-dimethyl-	√	√	√	√	√
SC	Sulfur dioxide	√	/	/	/	/
	Thiophene, tetrahydro−2-methyl-	√	√	√	√	√
	Thiophene, 3,4-dimethyl-	√	/	/	/	√
	Thiophene, 2,3-dimethyl-	√	√	√	√	√

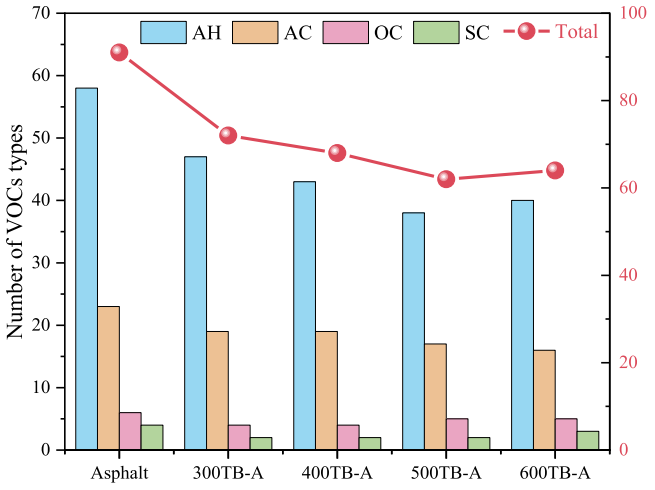

Fig. 13. Influence of TB on the number of VOCs types in asphalt fume.

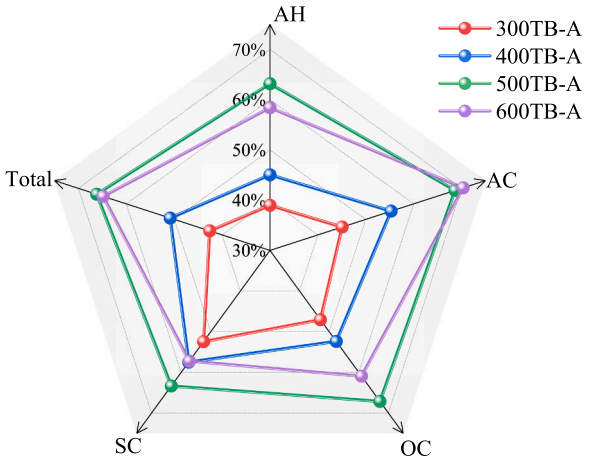

Fig. 14. Inhibition rate of VOCs components in asphalt by TB.

Table 4
Results of various pollutants in GC-MS.

	Asphalt ($\times 10^7$)	300TB-A ($\times 10^7$)	400TB-A ($\times 10^7$)	500TB-A ($\times 10^7$)	600TB-A ($\times 10^7$)
Total	25.74	14.78	12.65	8.70	9.06
AH	11.0	6.74	6.06	4.06	4.59
AC	13.7	7.54	6.13	4.30	4.07
OC	0.69	0.36	0.33	0.23	0.27
SC	0.30	0.14	0.13	0.11	0.13

conjugation effects facilitate more effective adsorption of aromatic pollutants.

In summary, the adsorption capacity of TB increased as the pyrolysis temperature rose, gradually improving the suppression effect on asphalt fume. This enhanced adsorption is likely due to the increasingly ordered and porous internal structure of the biochar at higher temperatures, which provided a larger BET surface area and improved its ability to capture various pollutants. The structural evolution of TB with pyrolysis temperature played a critical role in its effectiveness as an additive for reducing environmental pollution in asphalt applications. The ideal temperature for preparing tea branch biochar for asphalt fume adsorption was clearly identified as 500℃, at which TB exhibited balanced and efficient inhibition across AH, AC, OC, and SC components.

3.3. Adsorption mechanism of TB on asphalt fume

The adsorption performance of TB on asphalt fumes is primarily determined by its pore structure and surface chemical properties. The main adsorption mechanisms may have included the following components:

First, the characteristics of the pore structure of TB played a crucial role in its adsorption capacity. As the pyrolysis temperature increased, the BET surface area and porosity of biochar significantly expanded. These structural changes enhanced the adsorption capacity of biochar, providing more adsorption sites for volatile compounds emitted from asphalt. The pore structure captures asphalt fume molecules through physical forces such as van der Waals interactions. Biochar prepared at higher temperatures (500TB, 600TB) possessed a rich variety of pore sizes, effectively capturing fumes molecules of various molecular sizes, including both small and large fumes molecules. Additionally, the high pyrolysis temperature resulted in a more uniform and stable pore structure in biochar, further improving the adsorption efficiency for larger volatile molecules.

Second, the surface chemical properties of biochar changed with pyrolysis temperature, which also affected its adsorption performance. With the increase of pyrolysis temperature, the aromatic carbon framework in biochar gradually transforms into graphitization, exhibiting a higher degree of structural order and an expanded conjugated π-electron system. As the degree of graphitization of biochar increases, its surface hydrophilicity decreases, leading to the formation of more hydrophobic regions that enhance its adsorption capacity for nonpolar molecules such as alkanes and aromatics. Since many pollutants in

asphalt fume are nonpolar, hydrophobic interactions enable biochar to effectively adsorb and retain these compounds, thereby reducing their release. In addition, the aromatic carbon structure of biochar promotes π-π stacking interactions with aromatic compounds in asphalt fume. This interaction is a non-covalent attraction generated by the conjugated π-electron system in the aromatic rings, making it easier for aromatic pollutants to be adsorbed and fixed on the surface of biochar. Furthermore, as the degree of graphitization increases, the distribution of the π-electron cloud becomes more uniform, strengthening π-π interactions and enhancing the selective adsorption of aromatic pollutants by biochar.

At high temperatures (500–600℃), TB effectively enhanced its adsorption capacity for various pollutants in asphalt fume through these physical and chemical adsorption mechanisms, making TB an ideal material for reducing emissions from asphalt fume.

3.4. Physical properties of biochar modified asphalt

The effects of TB on the physical properties of asphalt are shown in Fig. 15. The results showed that biochar prepared at different pyrolysis temperatures had the same effect on the physical properties of asphalt, increasing the softening point and viscosity of asphalt, reducing penetration and ductility. Overall, TB had a relatively small impact on asphalt performance, with the impact of 600TB is greatest. This is because biochar particles act as a reinforcing framework within the asphalt, reducing its fluidity. Additionally, high-temperature biochar contains a significant amount of aromatic carbon structures, which can interact with the aromatic components of asphalt through π–π interactions, further restricting asphalt flow and thereby increasing its softening point and viscosity. Furthermore, the microporous and mesoporous structures of biochar can adsorb light oil fractions in asphalt. As these fluidizing components decrease, the asphalt becomes harder and more brittle, leading to lower penetration and reduced ductility, but this reduction is within an acceptable rang. To balance the effects of biochar on both asphalt fume adsorption performance and physical properties, 500TB is recommended as the preferred choice.

The penetration index (PI) is mostly utilized for indicating the temperature susceptibility. The PI calculation method is as follows:

$$PI = \frac{1952 - 500 \times \log(Pen) - 20 \times SP}{50 \times \log(Pen) - SP - 120}$$

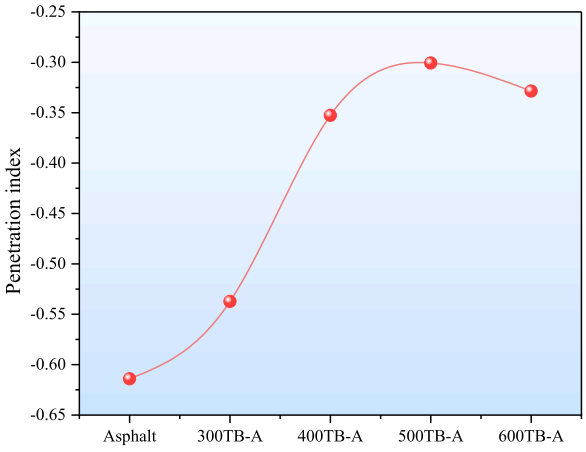

Fig. 16. Influence of TB on penetration index.

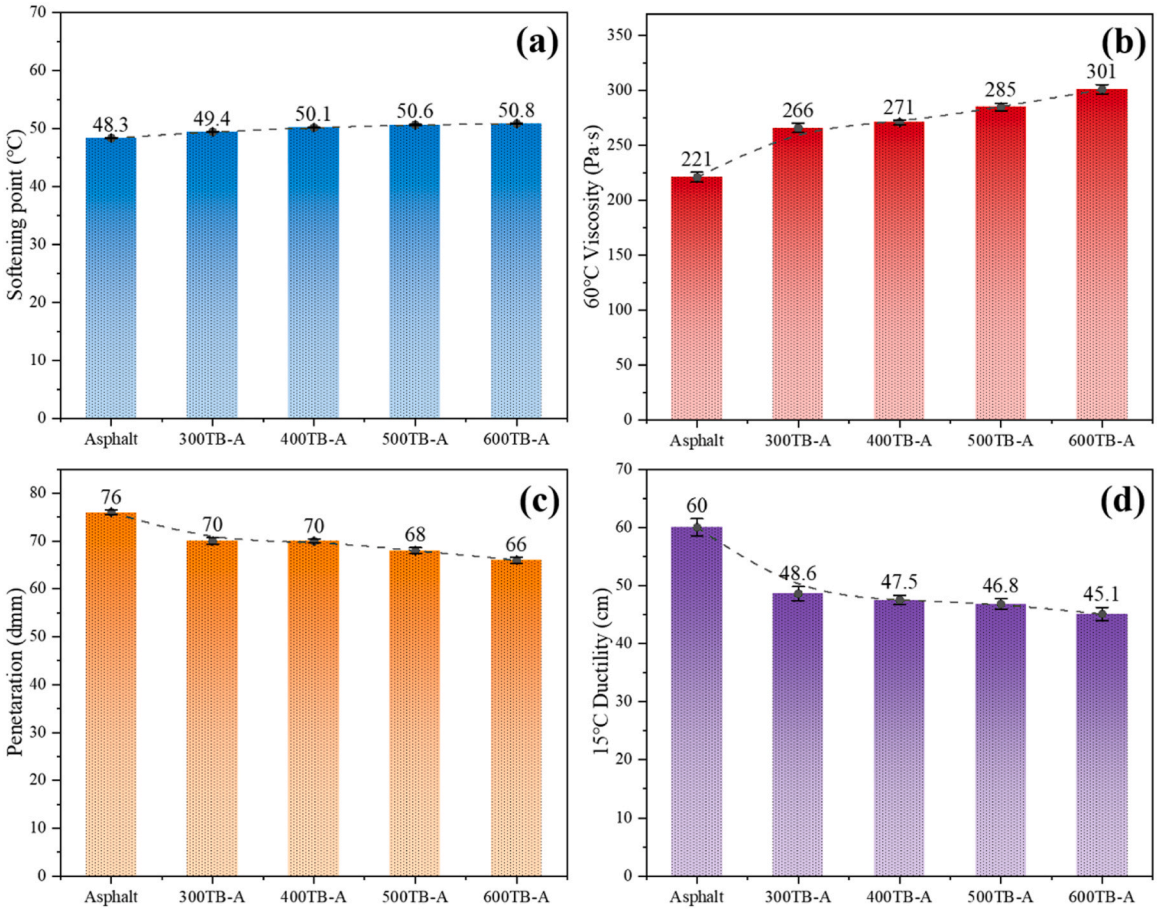

Fig. 15. Influence of TB on the physical properties of asphalt (a. softening point, b. 60℃ viscosity, c. penetration, d. 15℃ ductility).

Where SP represents softening point; Pen represents penetration.

As shown in Fig. 16, the incorporation of biochar led to changes in the PI. All modified asphalts exhibited higher PI values compared to the base asphalt, indicating that biochar effectively reduced the temperature sensitivity of asphalt. The PI of the base asphalt was −0.61, whereas the 500TB-A sample exhibited the highest PI at −0.30. This suggests that the 500TB-A sample became stiffer, enhancing its resistance to low-temperature cracking and high-temperature deformation during storage.

3.5. Economic feasibility

The application of TB in asphalt shows promising environmental benefits; however, the pyrolysis process of biochar involves additional energy consumption, making it necessary to estimate the associated costs. Given the excellent adsorption performance of 500TB, a brief feasibility analysis of its production was conducted in this study, as detailed below:

Key parameters and assumptions:

※ The specific heat capacity of lignocellulosic materials is approximately 1.4 kJ/(kg·℃) [39].
※ The thermal-to-electric conversion efficiency of industrial pyrolysis furnaces typically ranges from 60 % to 80 %, with 70 % used in this calculation.

1. Heating Phase (25℃ → 500℃)

When the heating rate is 15 ℃/min, the heating process needs to last for about 32 minutes.

The required heat energy:

$$Q_1 = m \bullet c \bullet \Delta T = 1000kg \times 1.4kJ/(kg/℃) \times 475℃ = 665000kJ$$

Converting to electrical energy (considering 70 % efficiency):

$$E_1 = \frac{665000}{3.6 \times 0.7} \approx 263889Wh \approx 263.9kWh$$

2. Temperature Holding Phase (500℃ for 2 hours)

Assuming furnace heat loss power is 30 % of heating power.

Heating power:

$$P_1 = \frac{Q_1}{t \times 3.6} = \frac{665000}{32 \times 60 \times 3.6} \approx 96.2kW$$

Holding power:

$$P_2 = 0.3 \times 96.2 \approx 28.9kW$$

Energy consumption during 2-hour holding phase:

$$E_2 = 28.9kW \times 2h = 57.8kWh$$

3. Endothermic Pyrolysis Reaction

The pyrolysis of wood absorbs approximately 400–600 kJ/kg, assuming an average of 500 kJ/kg:

$$E_3 = \frac{1000kg \times 500kJ/kg}{3.6 \times 0.7} \approx 198.4kWh$$

4. Total Energy Consumption Calculation:

$$E_{total} = E_1 + E_2 + E_3 = 520.1kWh$$

Based on industrial electricity price of China (0.6–0.9 CNY/kWh), the electricity cost of pyrolyzing one ton of biomass is approximately 312–468 CNY. As tea stalks are agricultural waste generated during tea harvesting and have a low price. According to the purchase price of tea stalks in this article, the estimated cost of raw materials for one ton of tea stalk is 1000 CNY. Consequently, the pyrolysis cost for one ton of tea stalks is estimated to be between 1312 and 1468 CNY. At a pyrolysis temperature of 500 °C, the biochar yield is approximately 28 %, resulting in an estimated cost of 4686 to 5243 CNY per ton of tea branch biochar. When the TB dosage is 1 % by weight in asphalt, the additional cost of asphalt is only about 47–53 CNY per ton. We believe that the increase in cost can be considered marginal compared to the beneficial effects it brings to the environment.

4. Conclusions

This study systematically investigated the impact of pyrolysis temperature (300℃, 400℃, 500℃, 600℃) on the microstructure and compositional characteristics of tea stalk biochar (TB) and further examined its inhibitory effect on asphalt fumes. The specific conclusions are as follows:

1. As the pyrolysis temperature increased from 300℃ to 600℃, significant changes occurred in the microstructure of TB. SEM analysis revealed that pore structure of TB transformed from dense and low-porosity to a more porous. BET analysis showed that TB prepared at higher temperatures had a larger BET surface area, smaller average pore size, and a broader distribution of micro- and mesopores. FTIR and EA analyses indicated that biochar produced at higher pyrolysis temperatures exhibited higher C content and C/H ratio, while O content and O/C ratio decreased, with a more pronounced aromatization reaction in the biochar.
2. The addition of 1 % TB significantly reduced the fumes emissions from asphalt. 300TB decreased VOCs by 37.1 %, H_2S by 48.5 %, SO_2 by 53.4 %, and NO_x by 48.3 %. With rising pyrolysis temperatures, the inhibitory efficiency progressively increased, with 500TB reducing VOCs by 68.6 %, H_2S by 87.5 %, SO_2 by 81.4 %, and NO_x by 75.9 %. The VOC suppression of 600TB was slightly lower than 500TB, possibly due to larger pore sizes in the 600TB structure causing some VOCs to escape.
3. GC-MS analysis indicated that VOCs emitted from asphalt could be categorized as AH, AC, OC, and SC, accounting for 42.9 %, 53.3 %, 2.7 %, and 1.2 % of the total pollutants, respectively. TB significantly reduced both quantity and total emissions of VOCs in asphalt fumes, with 500TB showing the highest inhibition rate and demonstrating the most effective suppression performance. In 500TB-A, the total emission volume decreased by 66 % (29 types reduced), with AH reduced by 63 % (20 types reduced), AC by 69 % (6 types reduced), SC by 67.2 % (2 types reduced), and OC by 63.3 % (2 types reduced).
4. The adsorption performance of TB on asphalt fumes was primarily determined by its pore structure and surface chemical properties. As the pyrolysis temperature increased, the BET surface area and porosity of TB significantly expanded, providing more adsorption sites and enhancing the physical adsorption capacity for VOCs of varying molecular sizes. Meanwhile, the increased hydrophobicity and graphitization of TB not only facilitate its dispersion in asphalt but also enhance its adsorption affinity for pollutants due to the π-π stacking effect of the aromatic carbon structure.
5. Biochar restricts the mobility of asphalt molecules, resulting in an increase in softening point and viscosity, and a decrease in penetration and ductility; however, these changes are relatively minor. In addition, biochar improves the penetration index of asphalt, enhancing its resistance to low-temperature cracking and high-temperature deformation.

6. Based on an economic feasibility analysis, the biochar produced at 500 ℃ offers a more favorable balance between performance and energy efficiency. Therefore, 500TB is recommended as the preferred fume suppressant additive for asphalt applications.

5. Recommendations for future work

This study prepared tea stalk biochar with different structural characteristics at various pyrolysis temperatures and investigated its effect on asphalt fume emissions. The results indicated that the biochar produced at a pyrolysis temperature of 500°C exhibited excellent inhibitory effects on asphalt fume emissions. Since the physical, rheological, and aging properties of asphalt are key indicators in engineering applications, future research should further explore the impact of biochar on these properties of asphalt. Additionally, future research should explore whether blending tea stalk biochars produced at different pyrolysis temperatures can enhance asphalt fume adsorption. Furthermore, the influence of biomass composition and structure on biochar's adsorption performance for asphalt fumes warrants further investigation.

CRediT authorship contribution statement

He Yanheng: Methodology, Investigation. **Mao Sanpeng:** Methodology, Investigation. **Yu Jianying:** Formal analysis, Data curation. **Han Xiaobin:** Methodology, Investigation. **Xu Shi:** Formal analysis, Data curation. **Liu Quantao:** Formal analysis, Data curation. **Duan Hao:** Writing – review & editing, Writing – original draft, Data curation.

Declaration of Competing Interest

The authors declare that they have no known competing financial interests or personal relationships that could have appeared to influence the work reported in this paper

Acknowledgement

This work was supported by the Science and Technology Project of Petro China Co. Ltd (RLY-2023Y-03) and State Key Laboratory of Silicate Materials for Architectures (Wuhan University of Technology) (SYSJJ2024-19).

Data availability

Data will be made available on request.

References

[1] Q. Lu, C. Xin, M. Alamri, M. Alharthai, Development of porous asphalt mixture with bio-based epoxy asphalt, J. Clean. Prod. 317 (2021) 128404, https://doi.org/10.1016/j.jclepro.2021.128404.
[2] C. Verilhac, G. Barreto, L. Devès, F. Delfosse, S. Carlotti, T. Lebarbé, J. Le-Meins, Influence of laboratory aging and asphaltene content of asphalt on frictional coefficient by tribological analysis – a case study, Fuel 379 (2025) 133013, https://doi.org/10.1016/j.fuel.2024.133013.
[3] B. He, Y. Xiao, Y. Li, M. Fu, J. Yu, L. Zhu, Preparation and characterization of lignin grafted layered double hydroxides for sustainable service of bitumen under ultraviolet light, J. Clean. Prod. 350 (2022) 131536, https://doi.org/10.1016/j.jclepro.2022.131536.
[4] M. Mousavi, J. Emrani, J. Teleha, G. Jiang, B. Johnson, A. Shamshiripour, E. Fini, Health Risks of Asphalt Emission: State-of-the-Art Advances and Research Gaps, J. Hazard. Mater. 480 (2024) 136048, https://doi.org/10.1016/j.jhazmat.2024.136048.
[5] B. Zhou, G. Gong, Y. Liu, M. Guo, C. Wang, Technical and environmental performance assessment of VOCs inhibited asphalt binders and mixtures, Transp. Res. Part D: Transp. Environ. 124 (2023) 103931, https://doi.org/10.1016/j.trd.2023.103931.
[6] Y. Boom, M. Enfrin, D. Xuan, S. Grist, D. Robert, F. Giustozzi, Laboratory evaluation of PAH and VOC emission from plastic-modified asphalt, J. Clean. Prod. 377 (2022) 134489, https://doi.org/10.1016/j.jclepro.2022.134489.
[7] R. Wu, Y. Xiao, P. Zhang, J. Lin, G. Cheng, Z. Chen, R. Yu, Asphalt VOCs reduction of zeolite synthesized from solid wastes of red mud and steel slag, J. Clean. Prod. 345 (2022) 131078, https://doi.org/10.1016/j.jclepro.2022.131078.
[8] M. Mousavi, S. Aldagari, E. Fini, Adsorbing volatile organic compounds within bitumen improves colloidal stability and air quality, ACS Sustain. Chem. Eng. 11 (2023) 9581–9594, https://doi.org/10.1021/acssuschemeng.3c00539.
[9] H. Kaur, R. Nsouli, G. Cerna, S. Shariati, M. Flores, E. Fini, L. Ackerman, investigation of earth-abundant metal salts for the inhibition of asphalt-derived volatile organic compounds, ACS Omega (2024), https://doi.org/10.1021/acsomega.4c02095.
[10] X. Zhang, Y. Xiao, Y. Long, Z. Chen, P. Cui, R. Wu, X. Chang, VOCs reduction in bitumen binder with optimally designed Ca(OH)2-incorporated zeolite, Constr. Build. Mater. 279 (2021) 122485, https://doi.org/10.1016/j.conbuildmat.2021.122485.
[11] Z. Lu, W. Sun, C. Li, W. Cao, Z. Jing, S. Li, X. Ao, C. Chen, S. Liu, Effect of granular activated carbon pore-size distribution on biological activated carbon filter performance, Water Res. 177 (2020) 115768, https://doi.org/10.1016/j.watres.2020.115768.
[12] Y. Boom, M. Enfrin, S. Grist, F. Giustozzi, Recycled plastic modified bitumen: evaluation of VOCs and PAHs from laboratory generated fumes, Sci. Total Environ. 832 (2022) 155037, https://doi.org/10.1016/j.scitotenv.2022.155037.
[13] Y. Long, S. Wu, Y. Xiao, P. Cui, H. Zhou, VOCs reduction and inhibition mechanisms of using active carbon filler in bituminous materials, J. Clean. Prod. 181 (2018) 784–793, https://doi.org/10.1016/j.jclepro.2018.01.222.
[14] P. Cui, S. Wu, Y. Xiao, M. Wan, P. Cui, Inhibiting effect of layered double hydroxides on the emissions of volatile organic compounds from bituminous materials, J. Clean. Prod. 108 (2015) 987–991, https://doi.org/10.1016/j.jclepro.2015.06.115.
[15] H. Wang, Q. Liu, S. Wu, Y. Lv, P. Wan, X. Gong, G. Liu, Study of synergistic effect of diatomite and modified attapulgite on reducing asphalt volatile organic compounds emission, Constr. Build. Mater. 400 (2023) 132827, https://doi.org/10.1016/j.conbuildmat.2023.132827.
[16] Z. Hua, H. Song, C. Zhou, Q. Xin, F. Zhou, W. Fan, S. Liu, X. Zhang, C. Zheng, Y. Yang, X. Gao, A promising catalyst for catalytic oxidation of chlorobenzene and slipped ammonia in SCR exhaust gas: Investigating the simultaneous removal mechanism, Chem. Eng. J. 473 (2023) 145106, https://doi.org/10.1016/j.cej.2023.145106.
[17] X. Chang, L. Wan, Y. Long, Y. Xiao, Y. Xue, Optimal zeolite structure design for VOC emission reduction in asphalt materials, Constr. Build. Mater. 366 (2023) 130227, https://doi.org/10.1016/j.conbuildmat.2022.130227.
[18] X. Chang, Y. Long, C. Wang, Y. Xiao, Chemical fingerprinting of volatile organic compounds from asphalt binder for quantitative detection, Constr. Build. Mater. 371 (2023) 130766, https://doi.org/10.1016/j.conbuildmat.2023.130766.
[19] Y. Lv, S. Wu, N. Li, P. Cui, H. Wang, S. Amirkhanian, Z. Zhao, Performance and VOCs emission inhibition of environmentally friendly rubber modified asphalt with UiO-66 MOFs, J. Clean. Prod. 385 (2023) 135633, https://doi.org/10.1016/j.jclepro.2022.135633.
[20] H. Huang, H. Zhang, D. Han, Ferrocene addition for suppression of hydrogen sulfide formation during thermal recovery of oil sand bitumen, Energy 230 (2021) 120744, https://doi.org/10.1016/j.energy.2021.120744.
[21] H. Liang, S. Song, X. Liu, F. Sun, Z. Cao, Y. Liu, Y. Ren, X. Li, Study on the inhibition effect and mechanism of basic zinc carbonate composite asphalt fumes suppressant, Constr. Build. Mater. 416 (2024) 135220, https://doi.org/10.1016/j.conbuildmat.2024.135220.
[22] Y. Xie, L. Wang, H. Li, L. Westholm, L. Carvalho, E. Thorin, Z. Yu, X. Yu, Ø. Skreiberg, A critical review on production, modification and utilization of biochar, J. Anal. Appl. Pyrolysis 161 (2022) 105405, https://doi.org/10.1016/j.jaap.2021.105405.
[23] K. Benis, A. Damuchali, J. Soltan, K. McPhedran, Treatment of aqueous arsenic – A review of biochar modification methods, Sci. Total Environ. 739 (2020) 139750, https://doi.org/10.1016/j.scitotenv.2020.139750.
[24] S. Bolan, S. Sharma, S. Mukherjee, M. Kumar, C. Rao, K. Nataraj, G. Singh, A. Vinu, A. Bhowmik, H. Sharma, A. El-Naggar, S. Chang, D. Hou, J. Rinklebe, H. Wang, K. Siddique, L. Abbott, M. Kirkham, N. Bolan, Biochar modulating soil biological health: a review, Sci. Total Environ. 914 (2024) 169585, https://doi.org/10.1016/j.scitotenv.2023.169585.
[25] H. Yang, S. Ye, Z. Zeng, G. Zeng, X. Tan, R. Xiao, J. Wang, B. Song, L. Du, M. Qin, Y. Yang, F. Xu, Utilization of biochar for resource recovery from water: a review, Chem. Eng. J. 397 (2020) 125502, https://doi.org/10.1016/j.cej.2020.125502.
[26] J. Cha, S. Park, S. Jung, C. Ryu, J. Jeon, M. Shin, Y. Park, Production and utilization of biochar: a review, J. Ind. Eng. Chem. 40 (2016) 1–15, https://doi.org/10.1016/j.jiec.2016.06.002.
[27] S. Krebsbach, J. He, S. Adhikari, Y. Olshansky, F. Feyzbar, L. Davis, T. Oh, D. Wang, Mechanistic understanding of perfluorooctane sulfonate (PFOS) sorption by biochars, Chemosphere 330 (2023) 138661, https://doi.org/10.1016/j.chemosphere.2023.138661.
[28] A. Kayiranga, Z. Luo, J. Ndayishimiye, F. Nkinahamira, E. Cyubahiro, T. Habumugisha, C. Yan, J. Guo, Z. Zhen, A. Tuyishimire, H. Izabayo, Insights into thallium adsorption onto the soil, bamboo-derived biochar, and biochar amended soil in Pomelo orchard, Biochar 3 (2021) 315–328, https://doi.org/10.1007/s42773-021-00095-1.
[29] X. Wang, Z. Guo, Z. Hu, H. Ngo, S. Liang, J. Zhang, Adsorption of phenanthrene from aqueous solutions by biochar derived from an ammoniation-hydrothermal method, Sci. Total Environ. 733 (2020) 139267, https://doi.org/10.1016/j.scitotenv.2020.139267.

[30] M. Zhang, G. Liu, R. Liu, J. Xu, W. Si, Y. Wei, High-efficient co-removal of copper and zinc by modified biochar derived from tea stalk: characteristics, adsorption behaviors, and mechanisms, J. Water Process Eng. 57 (2024) 104533, https://doi.org/10.1016/j.jwpe.2023.104533.
[31] U. Khalil, M. Bilal Shakoor, S. Ali, M. Rizwan, M. Nasser Alyemeni, L. Wijaya, Adsorption-reduction performance of tea waste and rice husk biochars for Cr(VI) elimination from wastewater, J. Saudi Chem. Soc. 24 (2020) 799–810, https://doi.org/10.1016/j.jscs.2020.07.001.
[32] S. Başakçılardan, S. Baran, Hydrothermal carbonization of various lignocellulosics: fuel characteristics of hydrochars and surface characteristics of activated hydrochars, Waste Manag. 100 (2019) 259–268, https://doi.org/10.1016/j.wasman.2019.09.021.
[33] X. Wang, C. He, L. Cui, Z. Liu, J. Liang, Effects of different expansion temperatures on the non-volatile qualities of tea stems, Foods 13 (2024) 398, https://doi.org/10.3390/foods13030398.
[34] H. Najafi, Z. Rezaei, M. Sobati, Thermal conversion potential of tea stems: experimental investigation, reaction mechanism, and kinetic modeling, Ind. Crops Prod. 207 (2024) 117753, https://doi.org/10.1016/j.indcrop.2023.117753.
[35] P. Duarah, D. Haldar, R. Singhania, C. Dong, A. Patel, M. Purkait, Sustainable management of tea wastes: resource recovery and conversion techniques (https://www.tandfonline.com/doi/abs/), Crit. Rev. Biotechnol. (2024), https://doi.org/10.1080/07388551.2022.2157701.
[36] A. Thanarasu, K. Periyasamy, K. Devaraj, P. Periyaraman, S. Palaniyandi, S. Subramanian, Tea powder waste as a potential co-substrate for enhancing the methane production in anaerobic digestion of carbon-rich organic waste, J. Clean. Prod. 199 (2018) 651–658, https://doi.org/10.1016/j.jclepro.2018.07.225.
[37] A. Zielińska, P. Oleszczuk, Evaluation of sewage sludge and slow pyrolyzed sewage sludge-derived biochar for adsorption of phenanthrene and pyrene, Bioresour. Technol. 192 (2015) 618–626, https://doi.org/10.1016/j.biortech.2015.06.032.
[38] B. Chen, D. Zhou, L. Zhu, Transitional adsorption and partition of nonpolar and polar aromatic contaminants by biochars of pine needles with different pyrolytic temperatures, Environ. Sci. Technol. 42 (2008) 5137–5143, https://doi.org/10.1021/es8002684.
[39] J. Wang, S. Hou, Z. Shen, J. Wen, C. Qi, Thermal characteristics and simulation of enzymatic lignin isolated from chinese fir and birch, Forests 13 (2022) 914, https://doi.org/10.3390/f13060914.